Supporting Information

Charge Transfer from Upconverting Nanocrystals to Semiconducting Electrodes: Optimizing Thermodynamic Outputs by Electronic Energy Transfer

Bing Shan[1], Ting-Ting Li[1,2], M. Kyle Brennaman[1], Animesh Nayak[1], Lei Wu[1], and Thomas J. Meyer*[,1]

[1] Department of Chemistry, University of North Carolina at Chapel Hill, Chapel Hill, North Carolina 27599, United States.

[2] Research Center of Applied Solid State Chemistry, Ningbo University, Ningbo, Zhejiang 315211, China.

Table of Contents

Figure S1 Synthetic scheme for the photoelectrodes---------- S3
Figure S2 Molar absorptivities of CdSe ---------- S4
Figure S3 TEM and size distribution of CdSe---------- S5
Figure S4 UV-Vis absorption spectrum of CdSe ---------- S6
Figure S5 Adsorption isotherm of CdSe---------- S7
Figure S6 Absorption difference spectra of An or Ph_2An---------- S8
Figure S7 Absorption difference spectra of CdSe ---------- S9
Figure S8 Molar absorptivities of An and Ph_2An----------S10
Figure S9 Photoluminescence of CdSe as a function of η_A ----------S11
Figure S10 Emission of CdSe on oxides linked by $-PhNH_2-$ ----------S12
Figure S11 Excitation spectra ----------S13
Figure S12 Upconversion efficiencies as a function of the surface coverage ratios ----------S14
Figure S13 Time-resolved emission of $^3CdSe^*$ in $-NH_2$-CdSe on Al_2O_3 ----------S15
Figure S14 Molar absorptivity changes of $CdSe^{+/0}$ and $CdSe^{0/-}$----------S16
Figure S15 Molar absorptivity changes of $An^{+/0}$ and $An^{0/-}$ ----------S17
Figure S16 Molar absorptivity changes of $Ph_2An^{+/0}$ and $Ph_2An^{0/-}$----------S18
Figure S17 Singlet excited state energy from the emission spectrum of An ----------S19
Figure S18 Singlet excited state energy from the emission spectrum of Ph_2An----------S20

Figure S19 ^{1}H NMR for An in DMSO-d_6 ---------- S21
Figure S20 ^{13}C NMR for An in DMSO-d_6 ---------- S22
Figure S21 ^{1}H NMR for Ph_2An in DMSO-d_6 ---------- S23
Figure S22 ^{13}C NMR for Ph_2An in DMSO-d_6 ---------- S24
Table S1 Surface binding constants and maximum surface coverages of CdSe ---------- S25
Table S2 Quenching efficiencies of $^{3}CdSe^{*}$ ---------- S25
Table S3 Injection efficiencies into TiO_2 or NiO by $^{1}An^{*}$ or $^{1}Ph_2An^{*}$ ---------- S25
Table S4 Ground and excited state potentials of the anthracenes ---------- S25
References ---------- S26

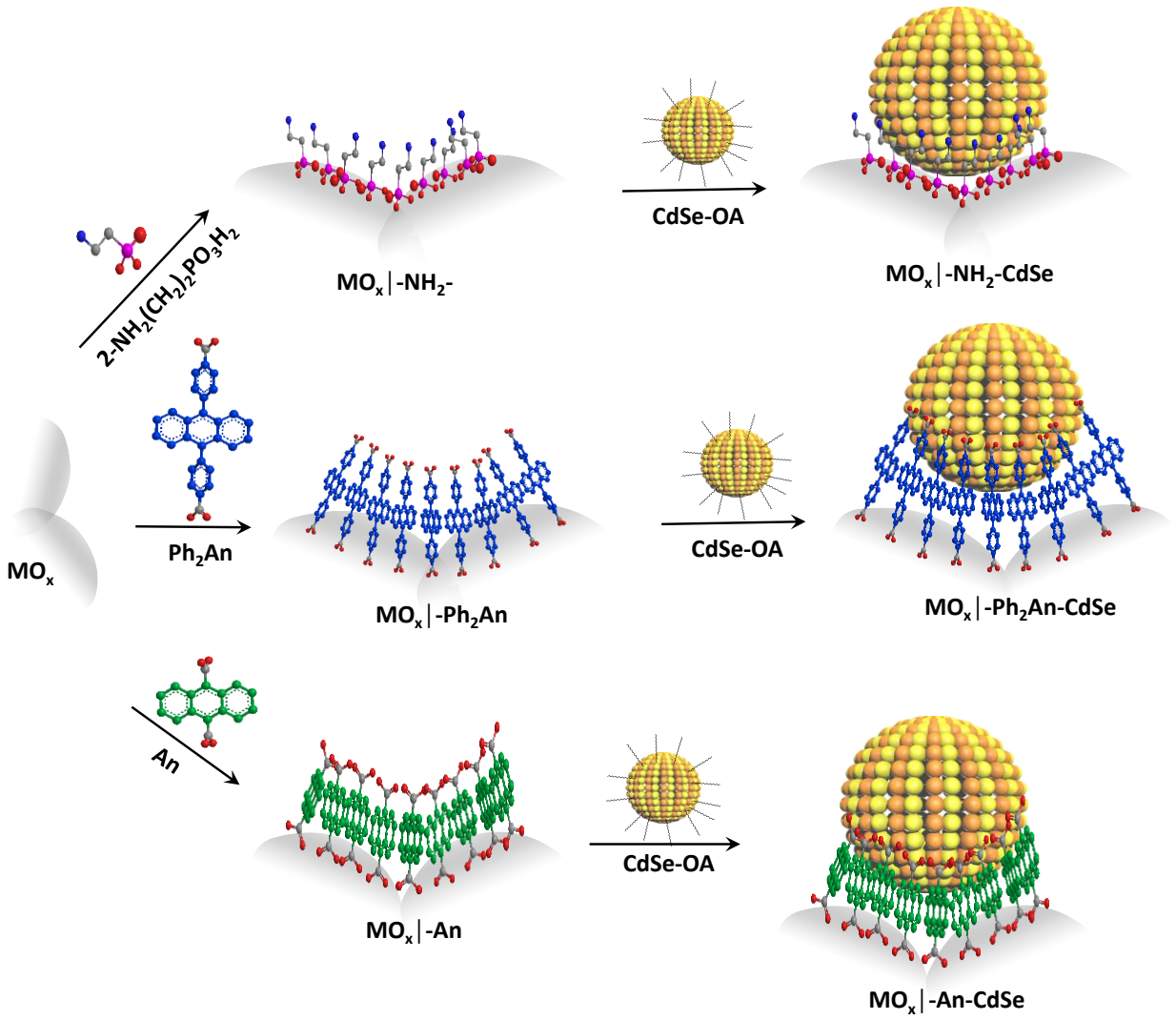

Figure S1. Synthetic scheme for the photoelectrodes.

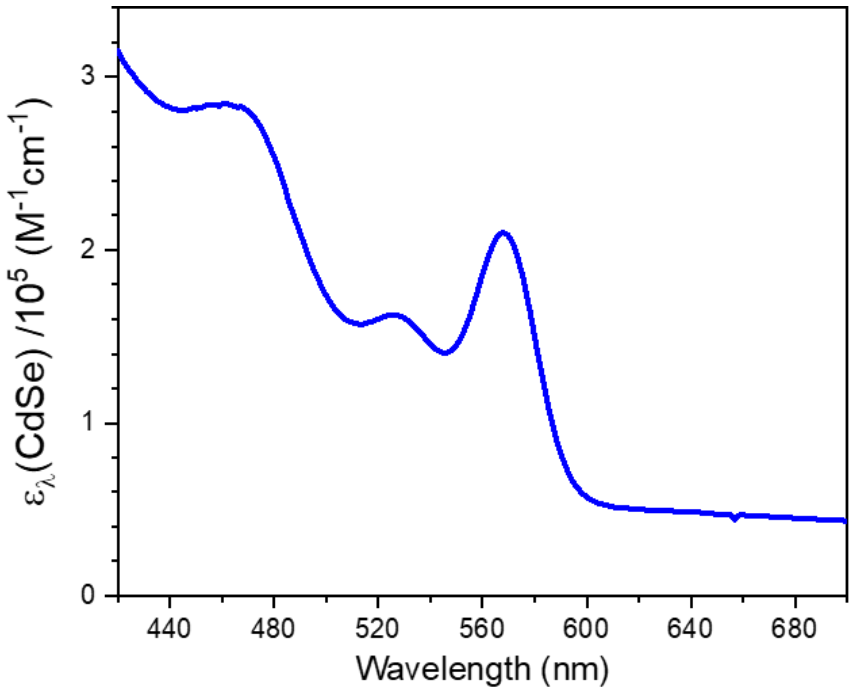

Figure S2. Molar extinction coefficients (ε_λ) of CdSe (in toluene).

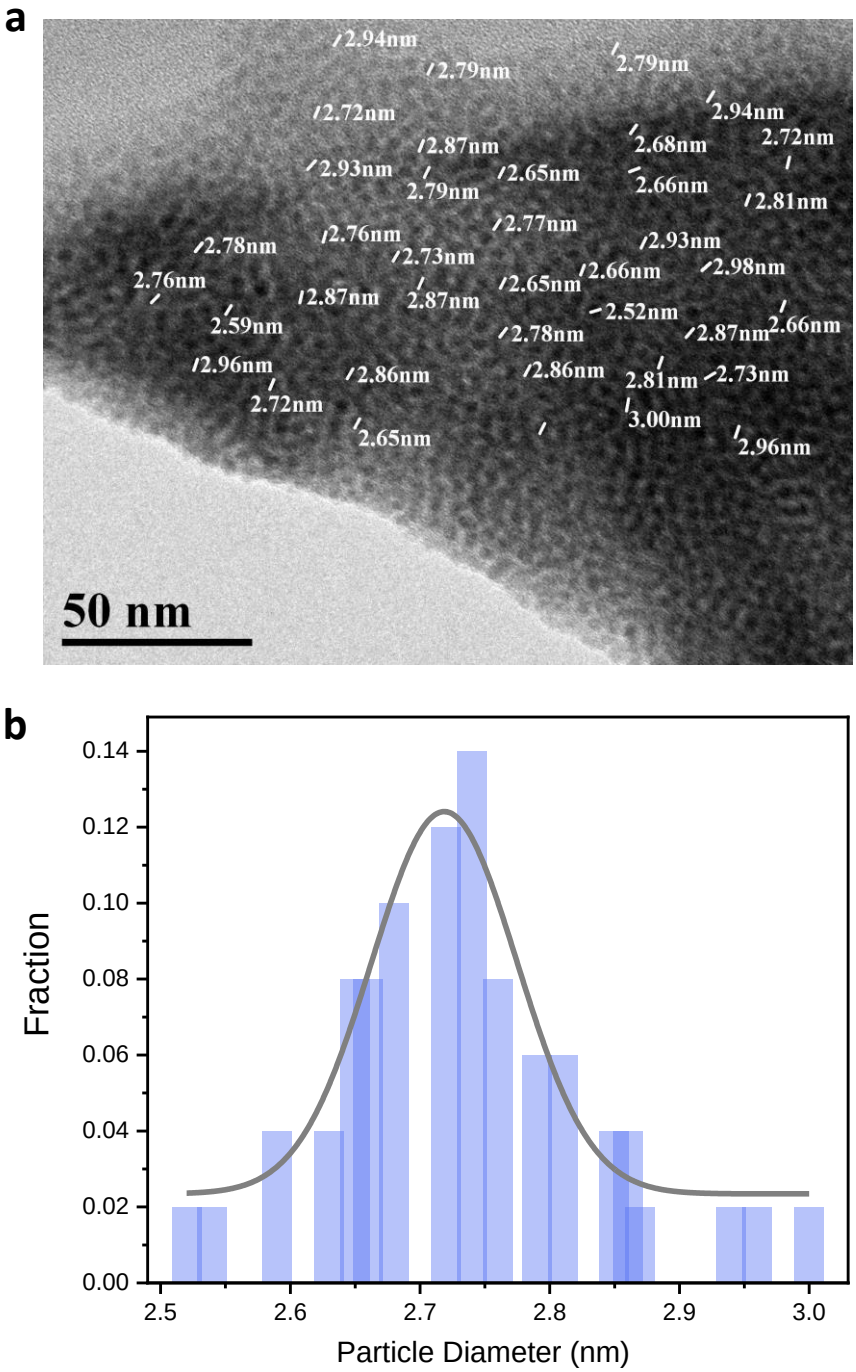

Figure S3. Transmission electron microscopy (TEM) images (a) and size distribution of the synthesized CdSe QDs.

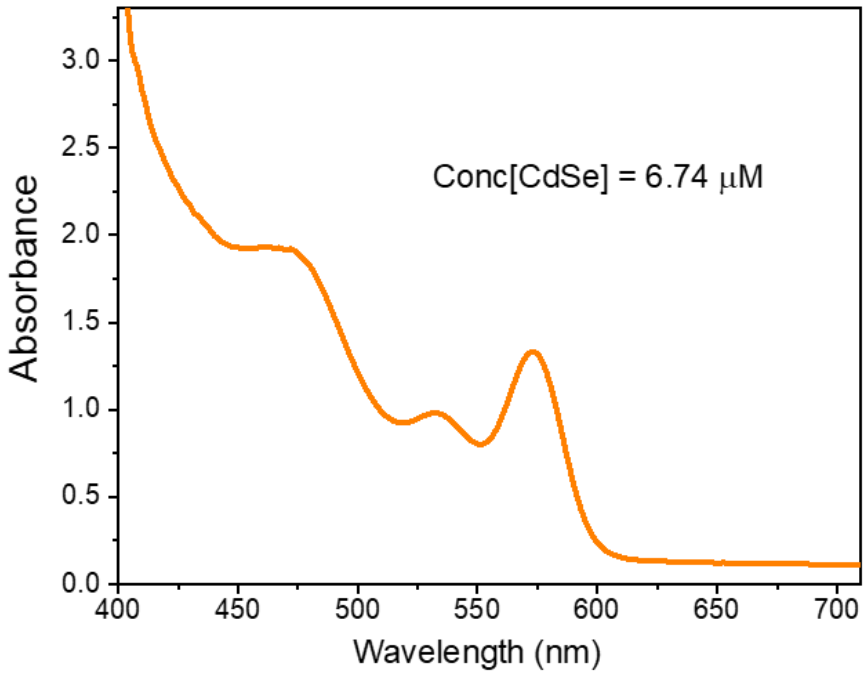

Figure S4. UV-Vis absorption spectrum of CdSe in toluene (6.74 μM).

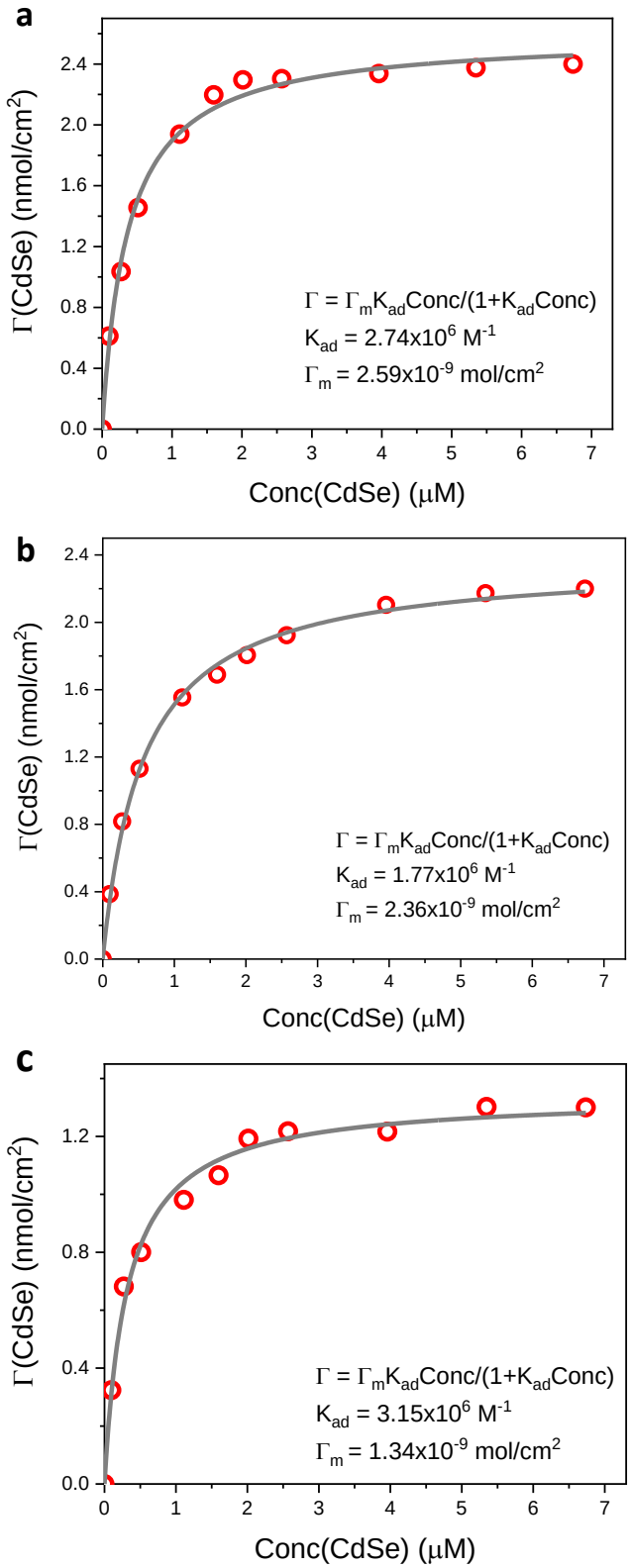

Figure S5. Adsorption isotherm of CdSe in the assembly -NH_2-CdSe on Al_2O_3 (**a**), TiO_2 (**b**) or NiO (**c**). All of the above isotherms were the average of two measurements.

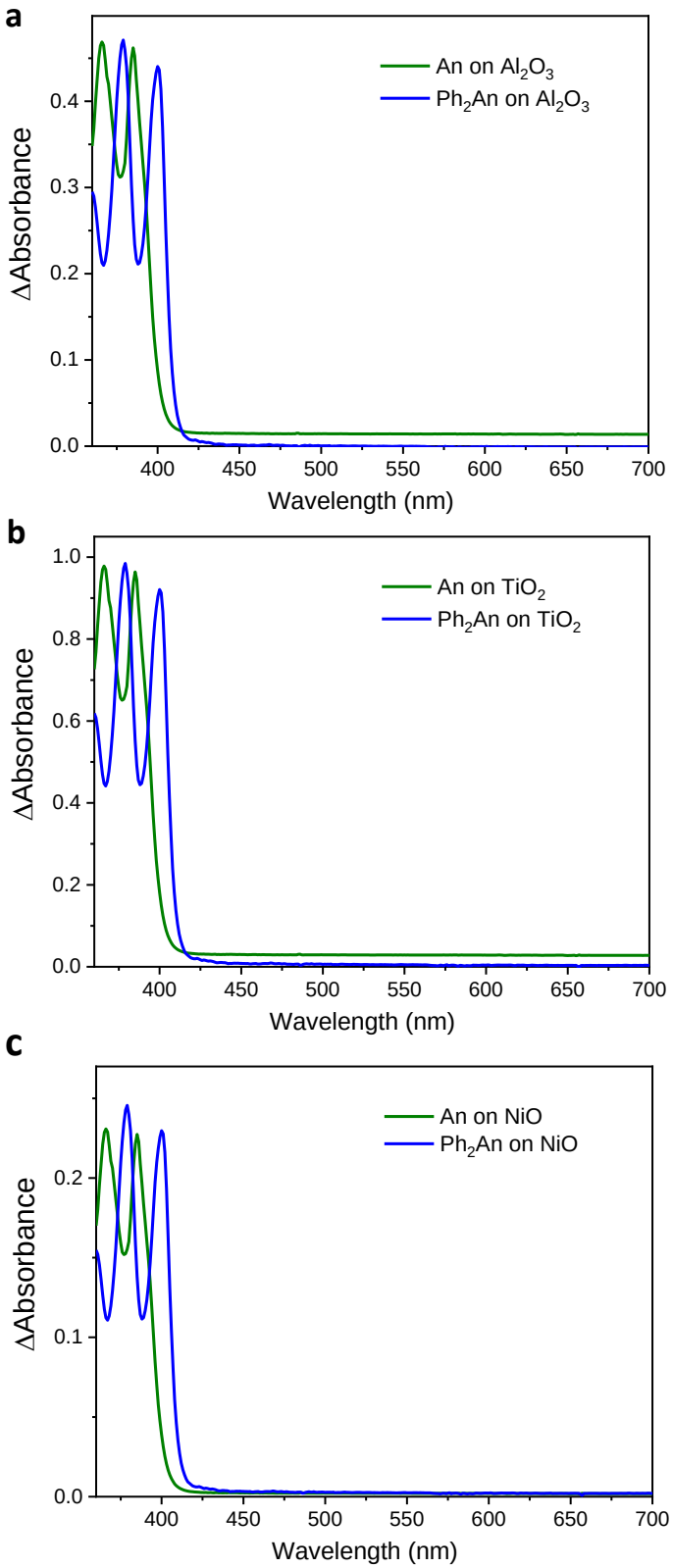

Figure S6. Absorption difference spectra upon addition of An or Ph_2An on Al_2O_3 (**a**), TiO_2 (**b**) or NiO (**c**).

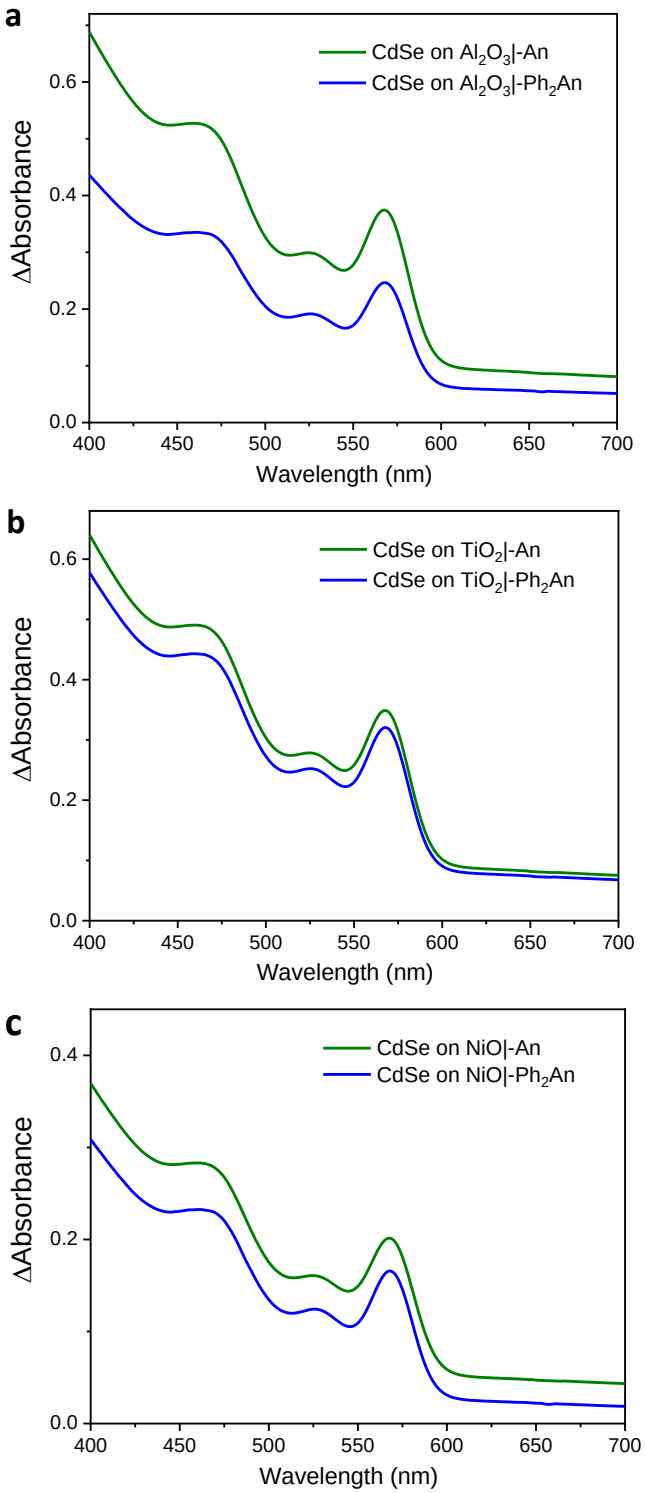

Figure S7. Absorption difference spectra upon addition of CdSe on the An or Ph_2An modified Al_2O_3 (**a**), TiO_2 (**b**) or NiO (**c**).

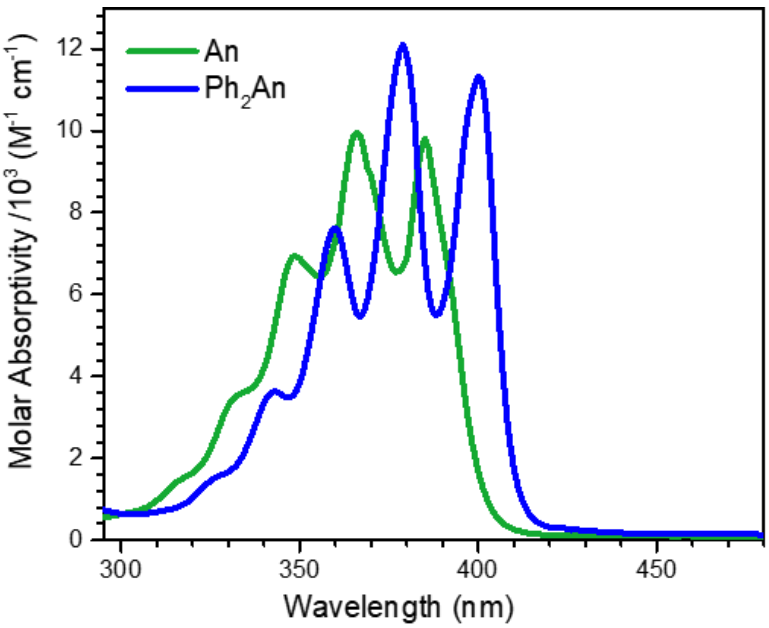

Figure S8. Molar absorptivities of An and Ph_2An.

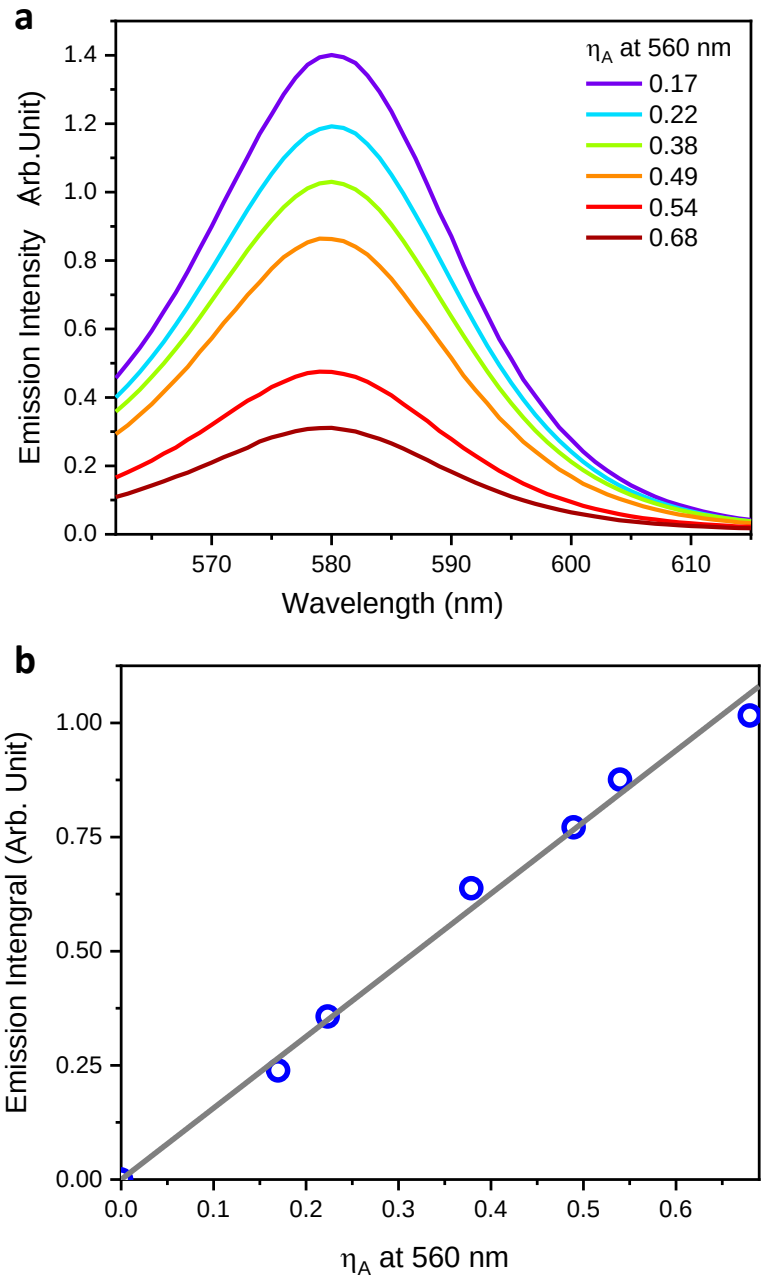

Figure S9. Photoluminescence (**a**) spectra of CdSe in Al_2O_3|-NH_2-CdSe excited at 560 nm as a function of the light absorption efficiencies (η_A) at 560 nm. (**b**) The linear relationship between the emission integrals and η_A at 560 nm.

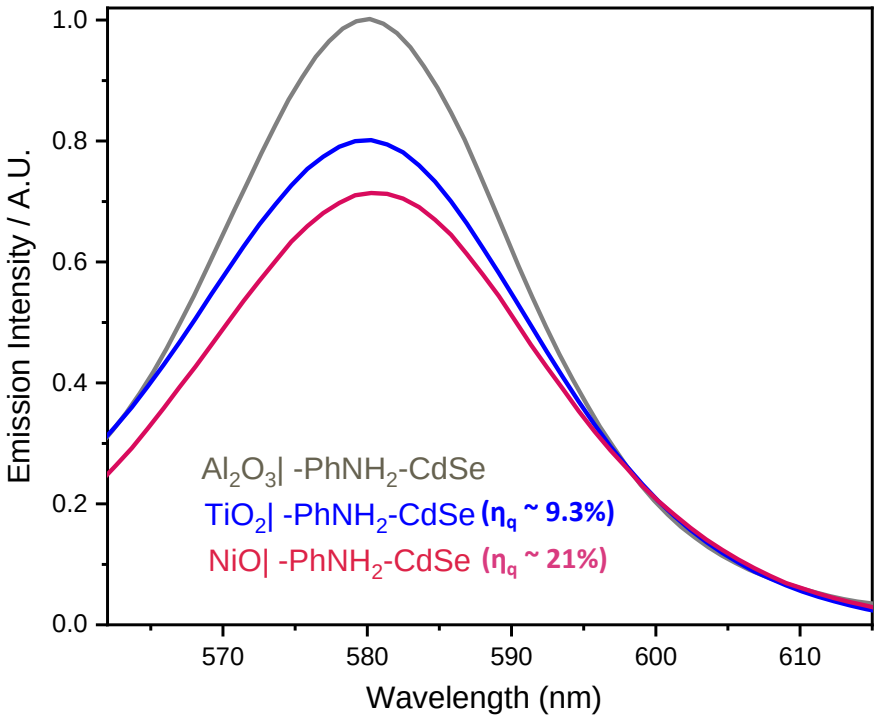

Figure S10. Steady-state emission following 560 nm excitation of CdSe on Al_2O_3 (gray), TiO_2 (blue) and NiO (red) linked by 4-aminobenzoic acid (abbreviated as -$PhNH_2$-). The surface coverages of CdSe were controlled at 2.0, 2.0 and 1.5 nmol/cm^2 for the Al_2O_3, TiO_2 and NiO samples, respectively. The emission intensities were normalized based on the light absorption efficiency ($\eta_A = 1\text{-}10^{-A_{560nm}}$) of each sample. The quenching (injection) efficiencies (η_q) based on the emission integrals of CdSe* are 9.3% and 21% for the TiO_2 and NiO samples, respectively.

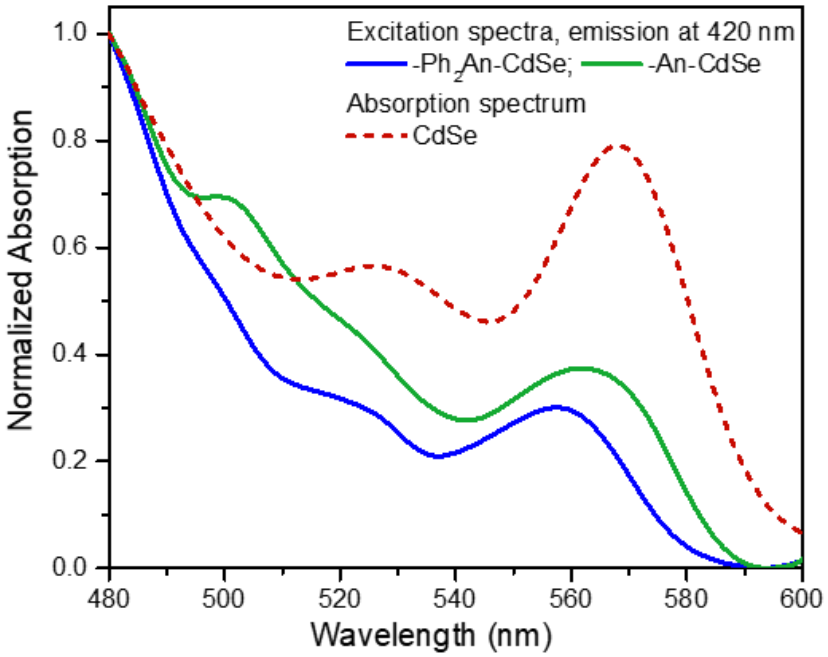

Figure S11. Excitation spectra for -An-CdSe (solid, green) and -Ph_2An (solid, blue) on Al_2O_3 and absorption spectrum for -NH_2-CdSe (dashed, red) on Al_2O_3. Emission was controlled at 410 nm.

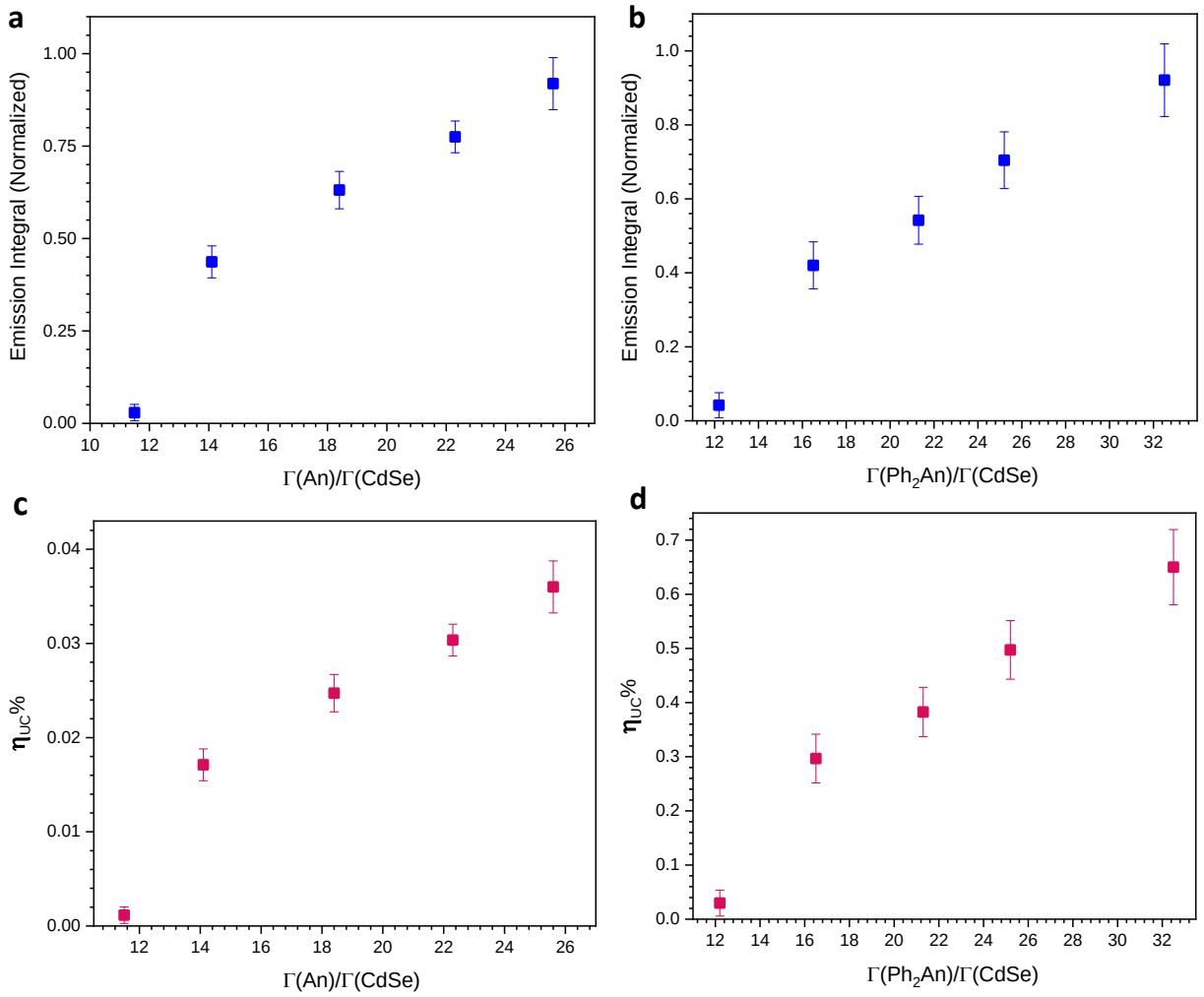

Figure S12. (**a**), (**b**) Upconversion emission integrals as a function of the surface coverage ratios of Γ(An)/Γ(CdSe) for Al_2O_3|-An-CdSe or Γ(Ph_2An)/Γ(CdSe) for Al_2O_3|-Ph_2An-CdSe, respectively. (**c**), (**d**) Upconversion efficiency (η_{UC}) as a function of the surface coverage ratios of Γ(An)/Γ(CdSe) for Al_2O_3|-An-CdSe or Γ(Ph_2An)/Γ(CdSe) for Al_2O_3|-Ph_2An-CdSe, respectively. Variations at Γ(An) and Γ(Ph_2An) were achieved by co-loading An/Ph_2An with the -NH_2- bridge.

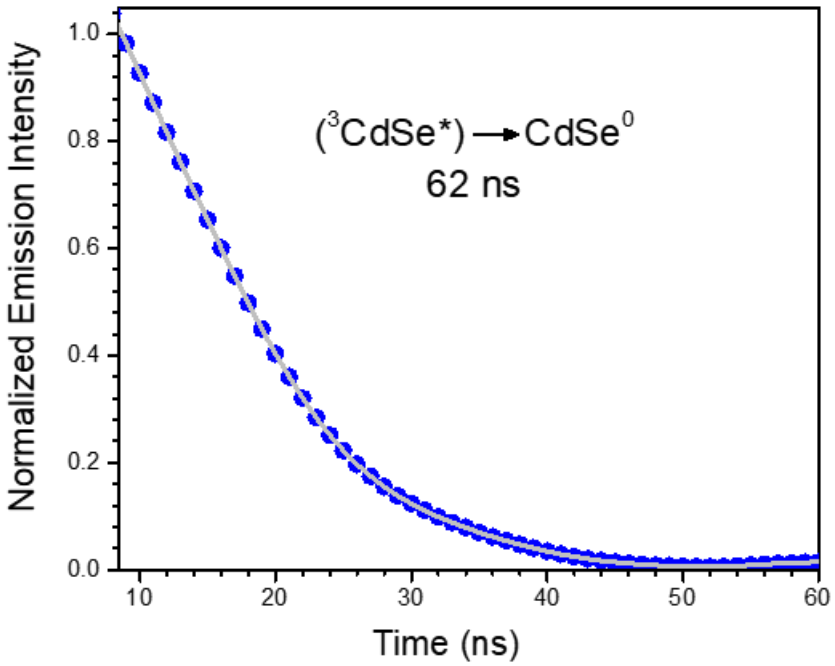

Figure S13. Time-resolved emission of ^{3}CdSe* at 580 nm following excitation of -NH_2-CdSe on Al_2O_3. The gray curve shows fitting by the KWW stretched exponential model, giving an excited state (τ_E) lifetime of 62 ns.

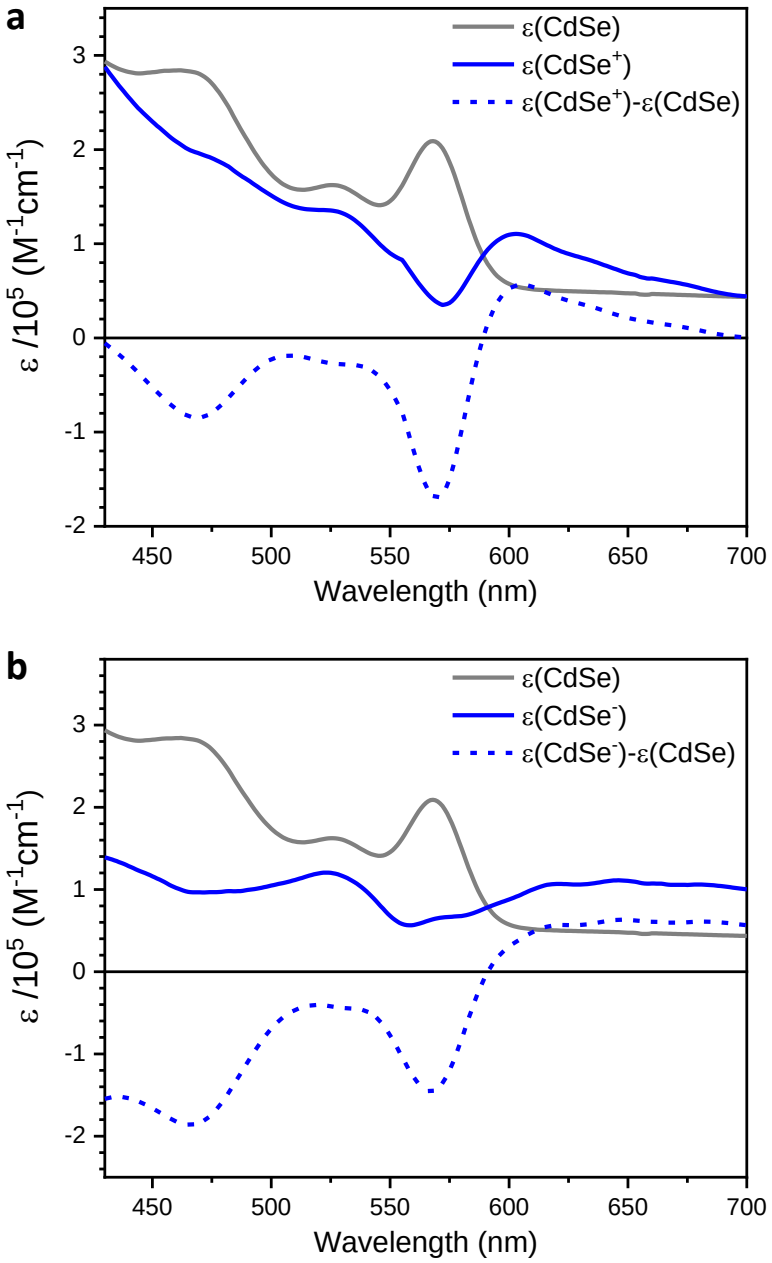

Figure S14. Molar absorptivities (ε) of $CdSe^+$ (**a**) and $CdSe^-$ (**b**) from spectroelectrochemistry of CdSe in -NH_2-CdSe on nanocrystalline ITO films. The spectral changes for $CdSe^+$ in ITO|-NH_2-$CdSe^+$ should result from reconstruction of the ligand-nanoparticle surface structure in the acetonitrile electrolyte.[1]

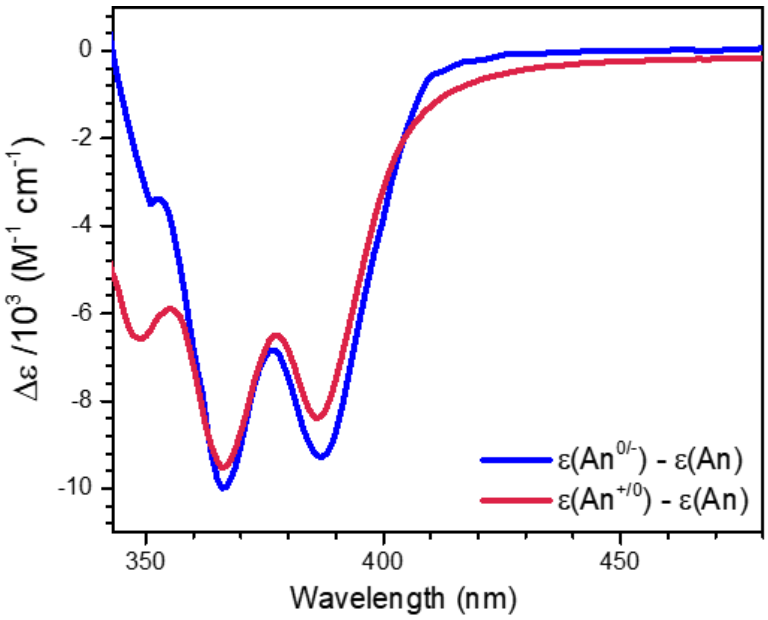

Figure S15. Molar absorptivity changes (Δε) of $An^{+/0}$ and $An^{0/-}$ from spectroelectrochemistry of An on NiO and TiO_2, respectively.

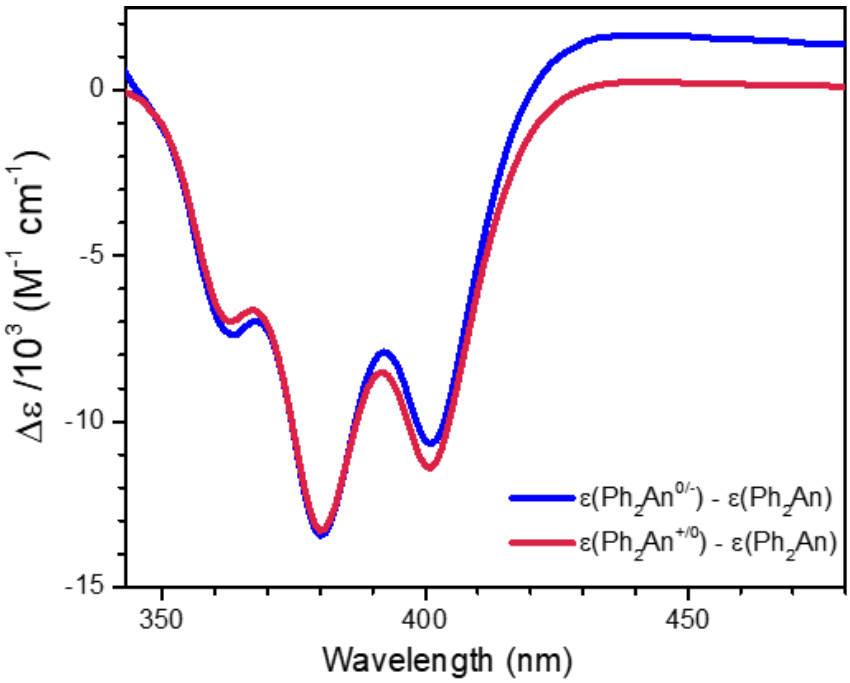

Figure S16. Molar absorptivity changes (Δε) of $Ph_2An^{+/0}$ and $Ph_2An^{0/-}$ from spectroelectrochemistry of Ph_2An on NiO and TiO_2, respectively.

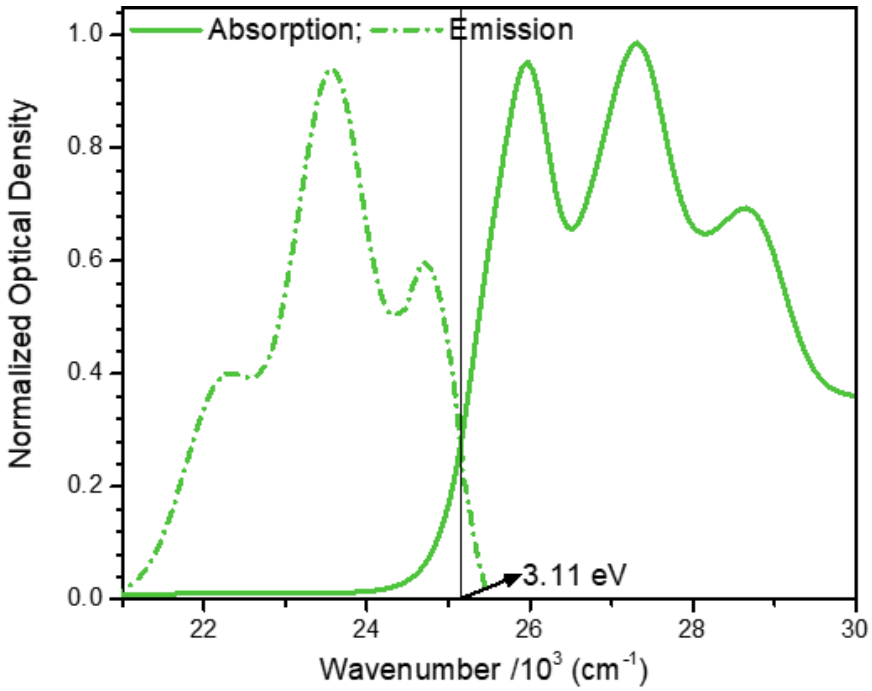

Figure S17. Normalized room temperature prompt fluorescence spectrum (dashed line) of An in DMSO-MeOH (1:1) excited at 390 nm with an intensity of 6 mW/cm^2 and its normalized absorption (solid line).

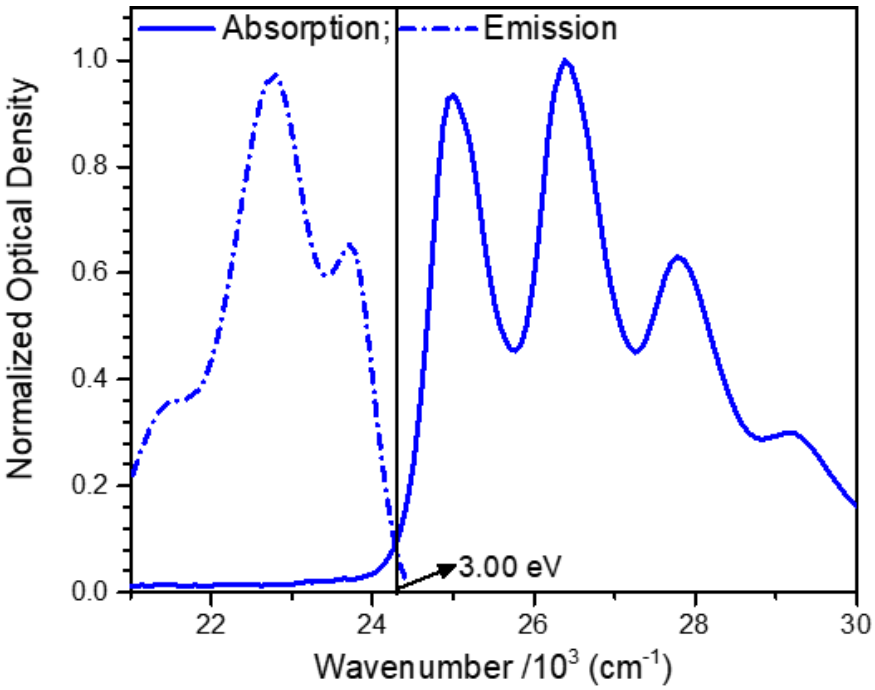

Figure S18. Normalized room temperature prompt fluorescence spectrum (dashed line) of Ph_2An in DMSO-MeOH (1:1) excited at 400 nm with an intensity of 6 mW/cm^2 and its normalized absorption (solid line).

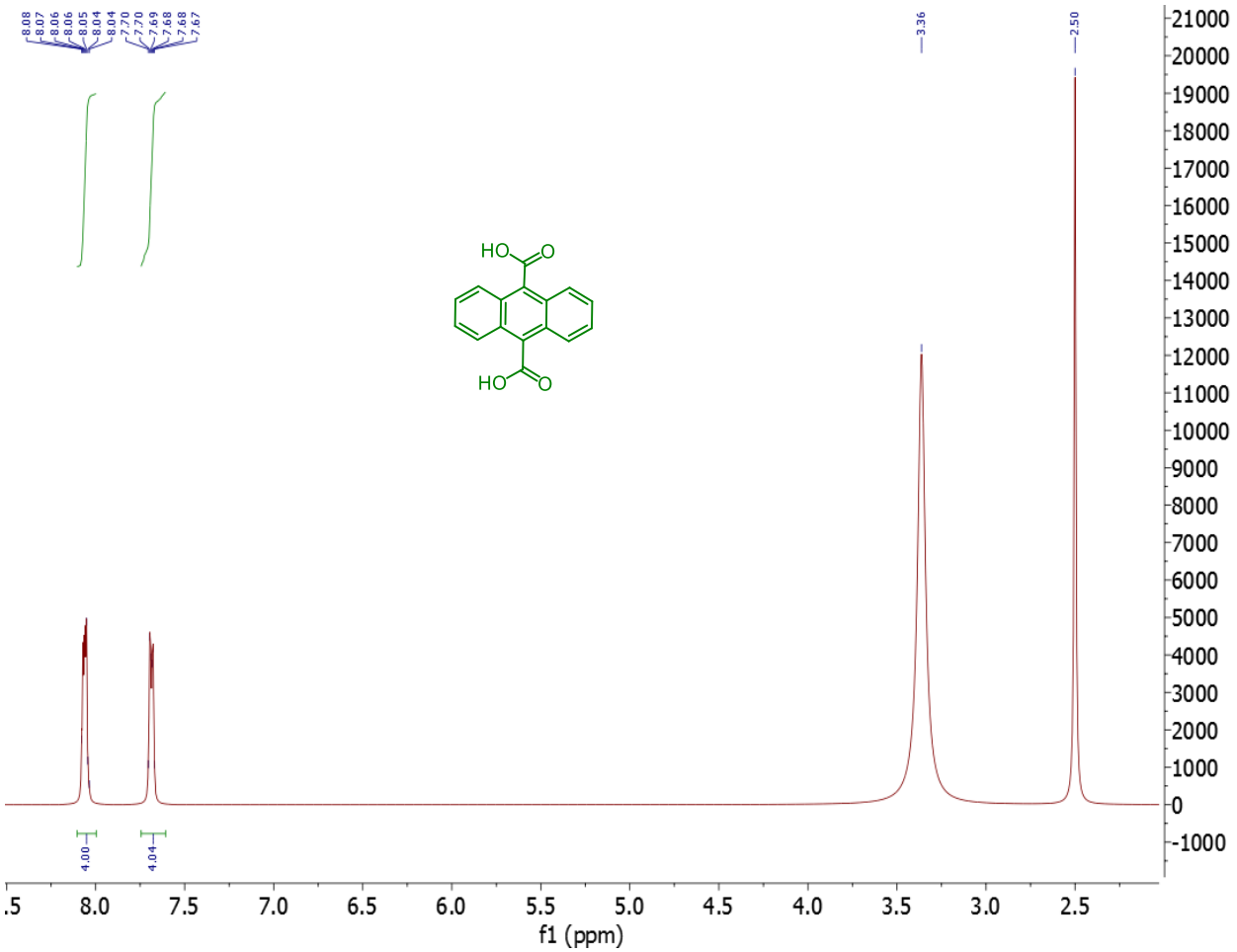

Figure S19. ^{1}H NMR for An in DMSO-d_6.

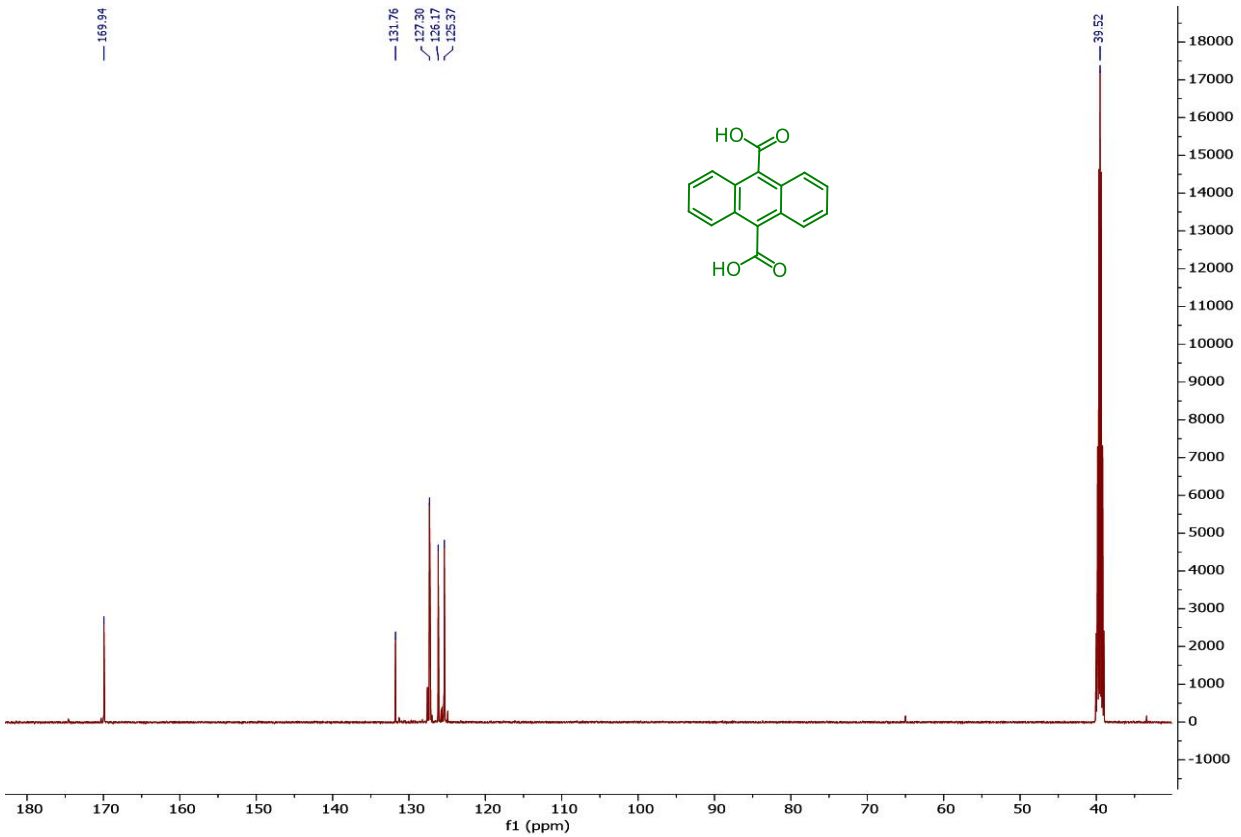

Figure S20. ^{13}C NMR for An in DMSO-d_6.

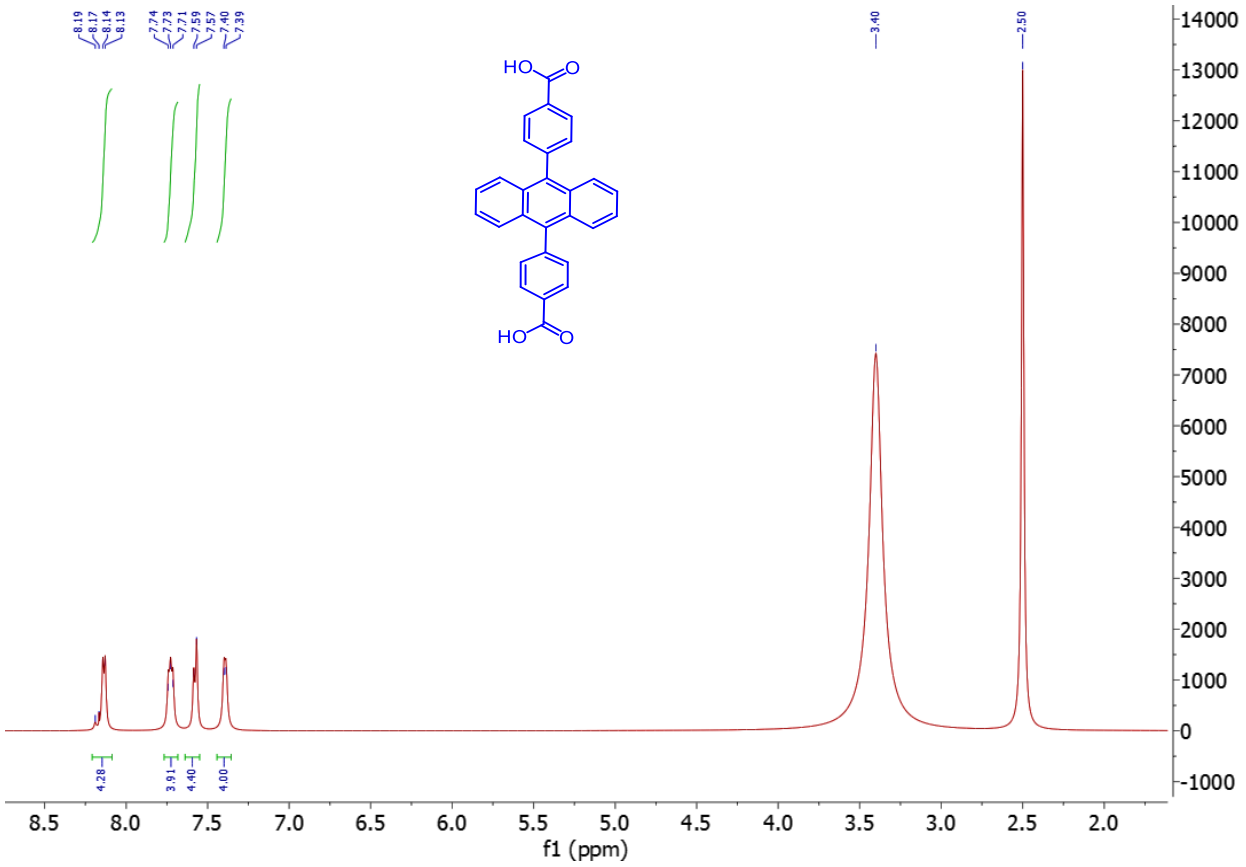

Figure S21. ^{1}H NMR for Ph_2An in DMSO-d_6.

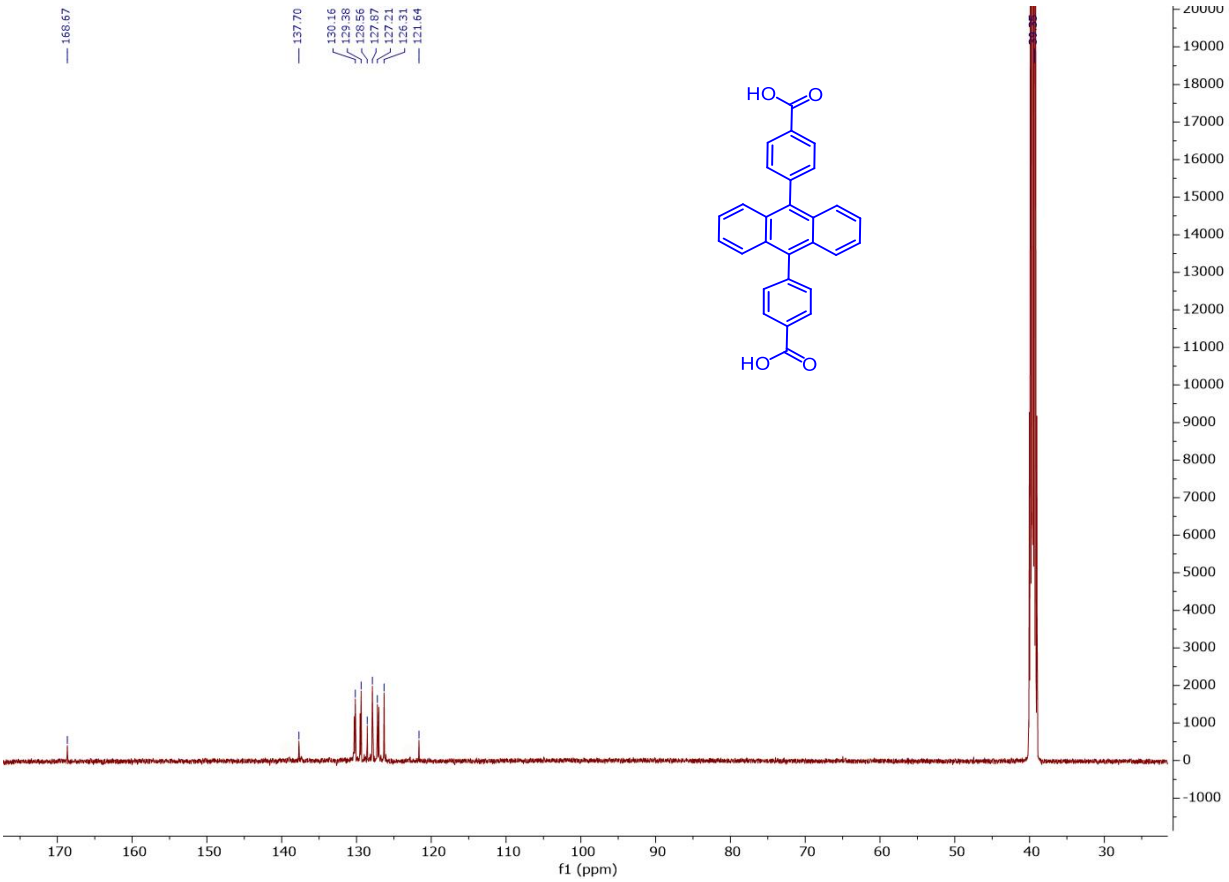

Figure S22. ^{13}C NMR for Ph_2An in DMSO-d_6.

Table S1. Surface binding constants (K_{ad}) and maximum surface coverages (Γ_m) of CdSe in -NH_2-CdSe on oxide films.

	K_{ad} (M^{-1})	Γ_m (nmol/cm^2)
Al_2O_3	2.74×10^6	2.59
TiO_2	1.77×10^6	2.36
NiO	3.15×10^6	1.34

Table S2. Quenching Yields (η_q) of ^{3}CdSe* by TiO_2, NiO, -An or -Ph_2An.

	TiO_2	NiO	-An	-Ph_2An
η_q	0.03	0.18	0.60	0.65

Table S3. Injection Efficiencies (η_{inj}) into TiO_2 or NiO by ^{1}An* or $^1Ph_2$An*.

	-An-CdSe	-Ph_2An-CdSe
TiO_2	0.63	0.58
NiO	0.72	0.50

Table S4. Ground and Excited State Potentials of the Anthracenes.

	GS [a]		ES3 [b]			ES1 [c]		
	$E_{GS}^{+/0}$/V	$E_{GS}^{0/-}$/V	ΔG_{ES3}/eV	$E_{ES3}^{+/0}$/V	$E_{ES3}^{0/-}$/V	ΔG_{ES1}/eV	$E_{ES1}^{+/0}$/V	$E_{ES1}^{0/-}$/V
An	1.31	-1.33	1.80	-0.49	0.47	3.11	-1.80	1.78
Ph_2An	1.33	-1.41	1.78	-0.45	0.37	3.00	-1.67	1.59

[a] Ground-state potentials determined by using a reported spectroelectrochemical method [2]. [b] Triplet excited state potentials obtained from ΔG_{ES3} [3-5] and the ground-state potentials. [c] Singlet excited state potentials obtained from ΔG_{ES1} (Figures S17, S18) and ground-state potentials.

References

1. Inerbaev, T. M.; Masunov, A. E.; Khondaker, S. I.; Dobrinescu, A.; Plamadă, A.-V.; Kawazoe, Y. *J. Chem. Phys.* **2009,** *131*, 044106.

2. Farnum, B. H.; Wee, K.-R.; Meyer, T. J. *Nat. Chem.* **2016,** *8*, 845-852.

3. Kepler, R. G.; Caris, J. C.; Avakian, P.; Abramson, E. *Phys. Rev. Lett.* **1963,** *10*, 400-402.

4. Laquai, F.; Wegner, G.; Im, C.; Büsing, A.; Heun, S. *J. Chem. Phys.* **2005,** *123*, 074902.

5. Baluschev, S.; Yakutkin, V.; Wegner, G.; Minch, B.; Miteva, T.; Nelles, G.; Yasuda, A. *J. Appl. Phys.* **2007,** *101*, 023101.